

The influence of transport model parameters on the isospin sensitive observables

Yingxun Zhang,^{1,2} P.Danielewicz,^{2,3} Zhuxia Li,¹ Hang Liu,⁴ Fei Lu,^{2,5} W.G.Lynch,^{2,3} and M.B.Tsang^{2,3}

¹*China Institute of Atomic Energy, P.O. Box 275 (10), Beijing 102413, P.R. China*

²*Joint Institute of Nuclear Astrophysics, Michigan State University, E. Lansing, MI 48824, USA*

³*National Superconducting Cyclotron Laboratory and Physics and Astronomy Department,
Michigan State University, East Lansing, MI 48824, USA*

⁴*Texas Advanced Computing Center, University of Texas, Austin, 78758 USA*

⁵*Department of Physics and State Key Laboratory of Nuclear Physics
and Technology, Peking University, Beijing 100871, P.R. China*

(Dated: March 22, 2019)

The influence of symmetry potential and in-medium NN cross section on the isospin sensitive observables of intermediate-energy heavy-ion collisions is explored with the ImQMD model. Focusing in the region above the Fermi energy, our results show that the symmetry potential plays a more important role on the experimental observables, double neutron to proton ratio and the isospin transport ratio R_t , than the in-medium nucleon-nucleon cross section. Since the copious production of intermediate mass fragments is a distinguishing feature of intermediate-energy heavy-ion collisions, we also examine the influence of cluster emission on the isospin transport ratio using different isospin tracers. The values of the isospin transport ratios with the tracer defined by the isospin asymmetry of the heaviest fragments with $Z \geq 20$ in the projectile region is greater than those obtained from lighter fragments. This phenomenon can be tested experimentally.

I. INTRODUCTION

Nuclear symmetry energy plays important roles on the properties of the nuclei and neutron star [1–5], and takes the form of a parabolic approximation

$$E_{\text{sym}} = S(\rho)\delta^2 \quad (1)$$

Here δ is the isospin asymmetry, ρ_n , ρ_p , are the neutron, proton densities, and $S(\rho)$ describes the density dependence of symmetry energy. Theoretical predictions on the density dependence of symmetry energy from microscopic nucleon-nucleon interactions show large uncertainties, especially for the supersaturation density [6, 7]. Constraining the density dependence of symmetry energy has become one of the main goals in nuclear physics and has stimulated many theoretical and experimental studies [7–28]. Heavy ion collisions (HIC) with neutron-rich nuclei provide a unique opportunity to study the density dependence of the symmetry energy in the laboratories because a large range of densities can be formed during the HICs. Up till now, the main strategy used to constrain the density dependence of the symmetry energy with heavy ion collisions was to measure the yields of emitted particles from neutron-rich or neutron-poor reaction systems. By comparing the experimental observables such as the neutron proton ratios and the isospin transport ratios to the predictions from transport model simulations, one obtains the constraints on the density dependence of symmetry energy [7, 26]. To fully understand the extracted constraints, we must know the influence of the other input parameters and the assumptions used in the transport codes.

Currently, most transport models are based either on the Uehling-Uhlenbeck approach to the Boltzmann equation or on the Quantum Molecular Dynamics approach. The two main ingredients of these transport models, the

nucleonic mean fields and nucleon-nucleon binary scattering cross sections, are not treated consistently with the same microscopic nucleon-nucleon interactions due to the difficulties on the non-equilibrium theory and numerical techniques. Consequently, all calculated observables depend on both the mean field and nucleon-nucleon binary collisions, especially for intermediate energy HICs. At low energies, the nucleon-nucleon collisions are absent and mean field govern the nucleon propagations. At high beam energies, the nucleon-nucleon collisions are frequent and mean free path become less ($\lambda < 2fm$). In addition, complex fragment production mechanism influences the isospin observables and the N/Z composition of the residues and emitted particles. As a microscopic dynamical n-body transport theory, formation of fragments is included in the Quantum Molecular Dynamics (QMD) type model without resorting to additional assumptions in the simulation of heavy ion collisions. However, the usual version of the QMD model [29] can not be used to study the influence of different density dependences of symmetry potential on the HIC observables due to absence of symmetry energy term. In the Improved QMD (ImQMD) model, the nucleons propagate under the nucleonic mean field derived from the Skyrme energy density functional and different forms of the density dependence of symmetry potential can be incorporated [30–33]. The ImQMD model has been very successful in describing the multiplicity of reaction products in intermediate energy HICs and has been used to understand the impact of cluster formation on neutron and proton ratios [30]. Recently, we have used the model to constrain the density dependence of the symmetry energy at sub-saturation density using chi-squared analysis on three experimental observables [26].

In this work, $^{112,124}\text{Sn} + ^{112,124}\text{Sn}$ at $E/A = 50\text{MeV}$ from central collisions to peripheral collisions are stud-

ied using the ImQMD model. The influences of density dependence of symmetry energy, in-medium nucleon-nucleon cross section and impact parameters on the isospin sensitive observables are investigated. We also discuss the influences of cluster emission on the isospin transport ratio. Since the main goal of this paper is to investigate the influences of various parameters used in the input for the transport model there is no attempt to obtain the best fit to the data as was done in ref[26].

II. MODEL DESCRIPTION AND REACTION PROPERTIES AT E/A=50MEV

In our investigations we use the Improved Quantum Molecular Dynamics code ImQMD05 of ref.[30–33]. Within the ImQMD05 model, the nucleonic mean fields acting on nucleon wavepackets are derived from a potential energy density functional where the potential energy U includes the full Skyrme potential energy with the spin-orbit term omitted:

$$U = U_\rho + U_{md} + U_{coul} \quad (2)$$

Here, U_{coul} is the Coulomb energy, while the nuclear contributions can be represented in local form with

$$U_{\rho,md} = \int u_{\rho,md} d^3r \quad (3)$$

and,

$$\begin{aligned} u_\rho = & \frac{\alpha}{2} \frac{\rho^2}{\rho_0} + \frac{\beta}{\eta+1} \frac{\rho^{\eta+1}}{\rho_0^\eta} + \frac{g_{sur}}{2\rho_0} (\nabla\rho)^2 \\ & + \frac{g_{sur,iso}}{\rho_0} (\nabla(\rho_n - \rho_p))^2 \\ & + \frac{C_s}{2} \left(\frac{\rho}{\rho_0}\right)^{\gamma_i} \delta^2 \rho + g_{\rho\tau} \frac{\rho^{8/3}}{\rho_0^{5/3}} \end{aligned} \quad (4)$$

where the asymmetry δ , and ρ_n and ρ_p are the neutron and proton density. In the present work, the symmetry potential energy density of the form $\frac{C_s}{2} \left(\frac{\rho}{\rho_0}\right)^{\gamma_i} \delta^2 \rho$ is used in transport model comparisons. The energy density associated with the mean-field momentum dependence is represented as

$$\begin{aligned} u_{md} = & \frac{1}{2\rho_0} \sum_{N_1, N_2} \frac{1}{16\pi^6} \int d^3p_1 d^3p_2 f_{N_1}(\vec{p}_1) f_{N_2}(\vec{p}_2) \\ & 1.57 [\ln(1 + 5 \times 10^{-4} (\Delta p)^2)]^2 \end{aligned} \quad (5)$$

f_N are nucleon Wigner functions, $\Delta p = |\vec{p}_1 - \vec{p}_2|$, the energy is in MeV and momenta are in MeV/c . The resulting interaction between wavepackets in Eq.(5) is described in Ref.[34]. All of the calculations use the above interactions, and the coefficients used in formula (4) are set to $\alpha = -356 MeV$, $\beta = 303 MeV$, $\eta = 7/6$, $g_{sur} = 19.47 MeV fm^2$, $g_{sur,iso} = -11.35 MeV fm^2$, $C_s = 35.19 MeV$, $g_{\rho\tau} = 0 MeV$. Appendix I discusses the influence on isospin observables when the isoscalar part of

the EoS obtained with Skyrme interactions is changed by the introduction of momentum dependence to Eq.(5).

Isospin-dependent in-medium nucleon-nucleon scattering cross sections in the collision term are assumed to be $\sigma_{nn/np}^* = (1 - 0.2\rho/\rho_0)\sigma_{nn/np}^{free}$ where the isospin dependent $\sigma_{nn/np}^{free}$ is taken from Ref [35] and isospin dependent Pauli blocking effects are the same as in [31–33]. Clusters are constructed by means of the minimum tree spanning method widely used in QMD calculations, in which particles with relative momentum smaller than P_0 and relative distance smaller than R_0 coalesce into one cluster. In the present work, the values of $R_0 = 3.5 fm$ and $P_0 = 250 MeV/c$ are employed.

From the adopted interaction in the ImQMD model, we construct the density dependence of symmetry energy for cold nuclear matter as follows:

$$S(\rho) = \frac{1}{3} \frac{\hbar^2}{2m} \rho_0^{2/3} \left(\frac{3\pi^2}{2} \frac{\rho}{\rho_0}\right)^{2/3} + \frac{C_s}{2} \left(\frac{\rho}{\rho_0}\right)^{\gamma_i} \quad (6)$$

where m is the nucleon mass and the symmetry coefficient $C_s = 35.19 MeV$. For this particular parameterization, the symmetry energy increases with decreasing γ_i at subsaturation density while the opposite is true for supranormal density. In general, the function is described as stiff-asy EoS for $\gamma_i > 1$, while soft-asy EoS describes the case when $\gamma_i < 1$. In the present work, calculations are performed using two representative cases of soft and stiff asy-EoS of $\gamma_i = 0.5$ and 2.0 and the region of interest is mainly the sub saturation density region.

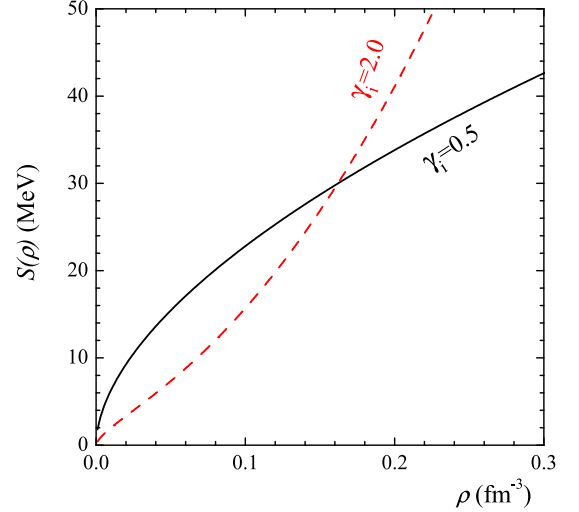


FIG. 1: (Color online) Symmetry energy per nucleon for cold nuclear matter plotted as a function of density for $\gamma_i = 0.5$ (solid line) and 2 (dashed line) used in ImQMD simulations (Eq.6).

Before discussing the influence of symmetry potential and in-medium NN cross sections on the HICs observables, we first show the dynamical process and fragment production mechanisms in Sn + Sn collisions at

$E/A = 50\text{MeV}$. Fig.2 (a) and (b) show the time evolution of the density contour plots for $^{124}\text{Sn} + ^{124}\text{Sn}$ at $E/A = 50\text{MeV}$ for $b = 0$ and 6fm from one typical event. The projectile and target touch around $50\text{fm}/c$ and nucleons start to transfer between projectile and target and the compressed region reaches the highest density around $100\text{fm}/c$ for both impact parameters. In central collisions ($b = 0\text{fm}$), the compressed reaction system expands to low density and multifragmentation occurs after $100\text{fm}/c$. In peripheral collisions ($b = 6\text{fm}$), the projectile/target residues separate around $150\text{fm}/c$ and the low-density neck is ruptured into fragments. The excited projectile/target residues move forward continuously along their paths after $150\text{fm}/c$. This suggests that the nucleon diffusion process in peripheral heavy ion collision finishes around $150\text{fm}/c$.

Figure 3 shows the charge (left panels) and mass (right panels) distributions of the reaction products for $^{112}\text{Sn} + ^{112}\text{Sn}$ at incident energy of 50MeV per nucleon for $b = 2, 6, 8\text{fm}$. The solid symbols are the results with $\gamma_i = 2.0$ and open circles are the results with $\gamma_i = 0.5$. The charge and mass distributions depend on the symmetry potential parameter γ_i . The multiplicity distribution of fragments obtained with $\gamma_i = 0.5$ is narrower than that obtained with $\gamma_i = 2.0$. In neutron-rich systems, the highest density in the overlap region is reached around $\gamma_i \sim 0.5$ and more compressional energy is stored for the soft-asy EoS case than that with stiff-asy EoS case. Higher compressed nuclear matter can expand to lower density and the reaction system with soft asy-EoS disintegrates into more fragments. Calculations show that the systems completely disintegrate into mainly nucleons for $\gamma_i \ll 0.5$.

For completeness, the contour plots of the multiplicity of fragments with charge Z as a function of its scaled rapidity $y/y_{beam}^{c.m.}$ for $^{112}\text{Sn} + ^{112}\text{Sn}$ for $b = 2, 6, 8\text{fm}$ are shown in Fig.4. In general, two ridges are observed in the rapidity distribution of fragment charge. Intermediate mass fragments with Z between 3 to 20 are formed from mid-rapidity to projectile/target rapidity sources formed in central collisions to peripheral collisions. In detail, the maximum charge of fragments in mid-rapidity decreases with increasing impact parameter b . The heaviest fragments have lost about 35% of their initial velocity for central collisions, and about 25%(10%) of their initial velocity for $b = 6\text{fm}$ ($b = 8\text{fm}$). The velocity loss of the heaviest fragments is closely related to the multiplicity of fragments formed below the normal density in HICs, and depends on the decelerating effects from the effective N-N interactions and nucleon-nucleon collision frequency. All of these features have been observed in experiments [18, 36].

III. INFLUENCE OF $S(\rho)$, $\sigma_{nn/np}^*$ AND IMPACT PARAMETERS b ON ISOSPIN OBSERVABLES

In order to estimate the uncertainties from the transport model simulations in constraining the density dependence of symmetry energy, the influence of symmetry potential, isospin dependence of in-medium NN cross-section, and impact parameters on the isospin sensitive observables are studied with the ImQMD model. In particular, we focus on the calculated results of the neutron to proton yield ratios as well as the isospin transport ratios (R_i). These two observables have been used extensively to provide constraints on the density dependence of symmetry energy at subnormal density [24,27].

A. Nucleon yield ratios

The symmetry potential, which is opposite in sign for proton and neutron, directly affects the emission of neutrons and protons. This fact has been recognized early on and has been studied quite intensively [21, 22, 26, 30]. However, due to low interaction with matter, neutrons are more difficult to measure and different types of detectors have to be employed to measure neutrons and protons. To minimize the effects of detector efficiencies, double ratios $DR(n/p) = R_{n/p(A)}/R_{n/p(B)} = (Y_n(A)/Y_p(A))/(Y_n(B)/Y_p(B))$ are normally constructed where $Y_n(A)$ and $Y_p(A)$ are the neutron and proton yields in system A . In Fig.5, the $DR(n/p)$ data from two collision systems $A = ^{124}\text{Sn} + ^{124}\text{Sn}$ and $B = ^{112}\text{Sn} + ^{112}\text{Sn}$ are plotted as solid stars in the left panel. The shaded regions in Fig.5 are the ImQMD results predicted with two different symmetry energy cases $\gamma_i = 0.5$ (upper shaded region) and 2.0 (lower shaded region). The impact parameter dependence is plotted in the right panel. In this study, the transverse emitted nucleons obtained with the angular cut of $70^\circ < \theta_{c.m.} < 110^\circ$, are selected as in Ref [20, 30]. From central to peripheral collisions, the $DR(n/p)$ for transverse emitted nucleons mainly relate to the information of symmetry energy of nuclear matter in the overlap region which contains the information of earlier stages of the collision. The observation that the $DR(n/p)$ ratios for the $\gamma_i = 0.5$ case are greater than that for $\gamma_i = 2.0$, is the same as that observed in other transport model predictions [21, 22]. At intermediate energy HICs, the emitted nucleons mainly come from the sub-normal density, where the symmetry energy is larger for smaller γ_i . Larger symmetry energy results in enhanced neutron emissions and larger values of the double ratios.

The symmetry potential parameter γ_i also influences the stability of initial nuclei. The initial nucleus becomes much less stable with decreasing γ_i due to the stronger repulsion of the neutrons on the surface of neutron-rich nuclei. The collision systems completely disintegrate into nucleons in the ImQMD simulations for very small values of $\gamma_i \ll 0.5$ and the $DR(n/p)$ ratios approach the limiting

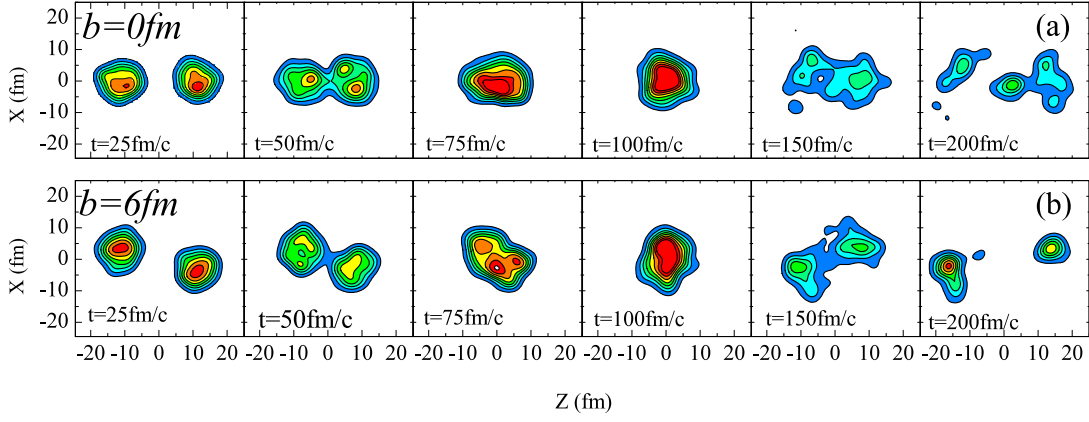


FIG. 2: (Color online) Time evolution of contour plots of nucleon density for reaction of $^{124}\text{Sn} + ^{124}\text{Sn}$ at $E/A=50\text{MeV}$ for $b=0$ (top panels) and 6 (bottom panels) fm.

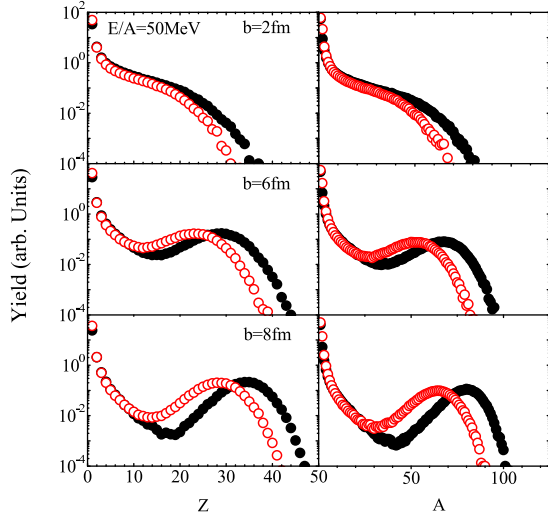


FIG. 3: (Color online) The charge (left panels) and mass (right panels) distributions for $^{112}\text{Sn} + ^{112}\text{Sn}$ at $b=2$ (top panels), 6 (middle panels), and 8 (bottom panels) fm. The solid symbols are for $\gamma_i = 2.0$ and open symbols are for $\gamma_i = 0.5$.

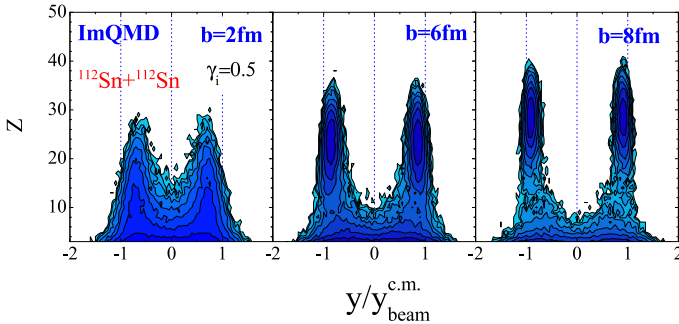


FIG. 4: (Color online) Contour plots of the multiplicity of fragments with charge Z as a function of their scaled rapidity $y/y_{\text{beam}}^{\text{c.m.}}$ for $^{112}\text{Sn} + ^{112}\text{Sn}$ at $E/A=50\text{MeV}$ for $b=2$ fm (left panel), 6 fm (middle panel), and 8 fm (right panel).

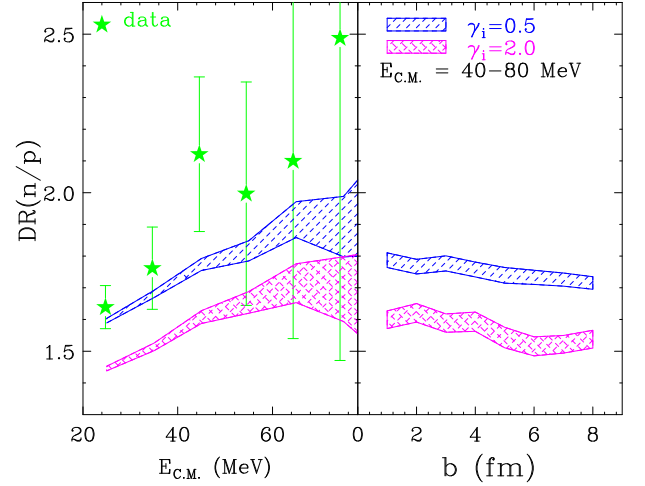


FIG. 5: (Color online) (Left panel) Double n/p yield ratios, $DR(n/p)$, from transverse emitted nucleons as a function of kinetic energy. The solid stars are data from ref. [20]. (Right panel) $DR(n/p)$ from transverse emitted high kinetic energy nucleons ($E_{\text{c.m.}} > 40\text{MeV}$) as a function of impact parameters. The upper shaded region is for $\gamma_i = 0.5$ and the lower shaded region is for $\gamma_i = 2.0$.

value of 1.2.

We investigate the impact parameter dependence of the $DR(n/p)$ ratios for emitted nucleons with $E_{\text{c.m.}} = 40 - 80\text{MeV}$, $\theta_{\text{c.m.}} = 70 - 110$ degree. The energy and angular gates are chosen to minimize sequential decays and cluster effects. The cuts also provide more robust coalescence-invariant quantities. As shown in the right panel of Fig.5, the impact parameter dependence is rather weak noting that there is a large zero-offset on the y-axis.

Similar to the symmetry potential, the isospin dependence of in-medium NN cross sections also plays an important role on the observables for heavy ion collisions

in the transport model. Here we test three kinds of in-medium NN cross sections on the DR(n/p) ratios: 1) normal case, $\sigma_{nn/np}^* = (1 - 0.2\rho/\rho_0)\sigma_{nn/np}^{free}$; 2) $\sigma_{nn/np}^* = \sigma_{nn/np}^{free}$; 3) isospin independent case, $\sigma_{nn}^* = \sigma_{pp}^* = \sigma_{np}^*$. We use the same energy and angular gate as the gated nucleons contain more information of the HICs at their earlier stage, and are more sensitive to the in-medium NN cross section. To remove the influence of the overall average NN cross section, we keep the total nucleon-nucleon collision number the same for cases 1) and 3). The calculated results of the DR(n/p) ratios are plotted in Fig.6. By comparing case 1 (open squares) and case 3 (solid circles), we can test the influence of the isospin dependence of the in-medium NN cross sections on the observables. The influence of $\sigma_{nn/pp}^*/\sigma_{nn/pp}^{free}$ can be investigated by comparing the DR(n/p) results obtained with case 1 (open squares) and case 2 (inverted triangles). DR(n/p) depends weakly on the in-medium NN cross section whether the soft ($\gamma_i = 0.5$) or stiff ($\gamma_i = 2$) symmetry potentials are used in the simulations. The reason is that the NN collision frequencies are suppressed by Pauli blocking at $E/A = 50\text{ MeV}$, and the different $\sigma_{nn/np}^*/\sigma_{nn/np}^{free}$ or $\sigma_{np}^*/\sigma_{nn}^*$ in the transport model do not lead to obvious differences in the DR(n/p) ratios. Thus, the isospin observable DR(n/p) ratio from Sn+Sn at $E/A = 50\text{ MeV}$ is a robust observable for constraining the density dependence of symmetry energy.

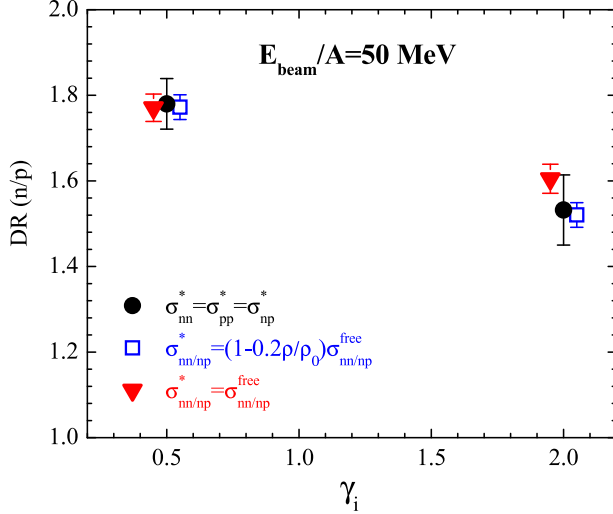


FIG. 6: (Color online) Effects of different in-medium NN cross section on DR(n/p) from transverse emitted high energy nucleons ($E_{c.m.} > 40\text{ MeV}$). The open squares are for isospin-dependent in-medium NN cross section with phenomenological formula (case 1 in text). The inverted triangles are for the free space NN cross section (case 2). The solid circles are for the isospin-independent in-medium NN cross section (case 3).

B. Isospin transport ratio R_i

In the case when the neutron to proton ratios differ greatly between projectile and target, there is a net neutron flux into the lower density neck region and isospin diffusion occurs. This isospin diffusion process, which depends on the magnitude of the symmetry energy, affects the isospin asymmetry of the projectile/target residues in peripheral HICs. The isospin transport ratio R_i has been introduced [14] to quantify the isospin diffusion effects,

$$R_i = \frac{2X - X_{AA} - X_{BB}}{X_{AA} - X_{BB}} \quad (7)$$

The subscripts A and B represent the neutron rich and neutron-poor nuclei, and $A = {}^{124}\text{Sn}$, $B = {}^{112}\text{Sn}$ in this work. The value of R_i is obtained through three reaction systems, $A + A$, $B + B$ and $A + B$ (or $B + A$), where X is an isospin observable. The non-isospin diffusion effects are minimized by scaling the isospin observables with the same observables from the symmetric collisions of the neutron-rich $A+A$ and neutron-deficient $B+B$ systems. Based on Eq.(7), one expects $R_i = \pm 1$ in the absence of isospin diffusion and $R_i \sim 0$ if isospin equilibrium is achieved. Eq.(7) also dictates that different observables, X , will give the same results if they are linearly related. In one experiment, X is taken as the isoscaling parameter, α , from the yield of the light particles near the projectile rapidity [14]. In the transport model [14, 15] based on the Boltzmann Uehling Uhlenbeck (BUU) approach, the isospin asymmetry δ of the projectile residues (emitting source) have been used to compute $R_i(\delta)$. The constraints on the density dependence of symmetry energy were obtained by comparing BUU predictions to the isospin diffusion data. This is possible only if the isoscaling parameters α are linearly related to the isospin asymmetry of the projectile residues. This has been shown both experimentally and theoretically [12, 18, 37] mainly in central collisions. In the BUU analysis, the projectile residues are defined with density greater than $0.05\rho_0$ and the center of mass velocity greater than half of the beam velocity [14]. The definition of a residue based on this criterion is not applicable in the ImQMD model as cluster process is introduced and fragments are produced. For the very central collision, there is no large residue.

ImQMD calculation shows that isospin diffusion for ${}^{124}\text{Sn} + {}^{112}\text{Sn}$ at $b = 6\text{ fm}$ stops around $150\text{ fm}/c$. The nucleons and fragments emitted at later stages do not give contributions to the isospin diffusion process, but their isospin contents should still be taken into account. To obtain the isospin transport ratios, we used three different isospin tracers to calculate the isospin transport ratios of Eq.(7). We simulated the collisions of four reaction systems ${}^{124}\text{Sn} + {}^{124}\text{Sn}$, ${}^{124}\text{Sn} + {}^{112}\text{Sn}$, ${}^{112}\text{Sn} + {}^{124}\text{Sn}$, ${}^{112}\text{Sn} + {}^{112}\text{Sn}$ at incident energy of 50 MeV per nucleon at different impact parameters.

In the first case, the isospin asymmetry of projectile residues (or emitting source) are constructed from the

emitted nucleons (N) and fragments (frag) with their velocity cut $v > 0.5v_{beam}^{c.m.}$ (Nearly identical results are obtained with higher velocity cut $v > 0.7v_{beam}^{c.m.}$). The left panel in Fig.7 shows the results of isospin transport ratios $R_i(X = \delta_{N,frag})$ (upright triangles) as a function of the impact parameters for two values of $\gamma_i = 0.5$ (open symbols) and 2.0 (closed symbols). In the second case, the residues are composed of all nucleons (including both bound and unbound nucleons) with their velocity cut at $v > 0.5v_{beam}^{c.m.}$. The inverted triangles $R_i(X = \delta_N)$ represent the results from this definition of residues. The isospin transport ratios constructed with these two tracers are very similar in values. R_i obtained with soft symmetry case ($\gamma_i = 0.5$) is smaller than those obtained with stiff symmetry potential case ($\gamma_i = 2.0$). This is consistent with the expectation that higher symmetry energy at subnormal density with $\gamma_i = 0.5$ leads to larger isospin diffusion effects (smaller R_i values).

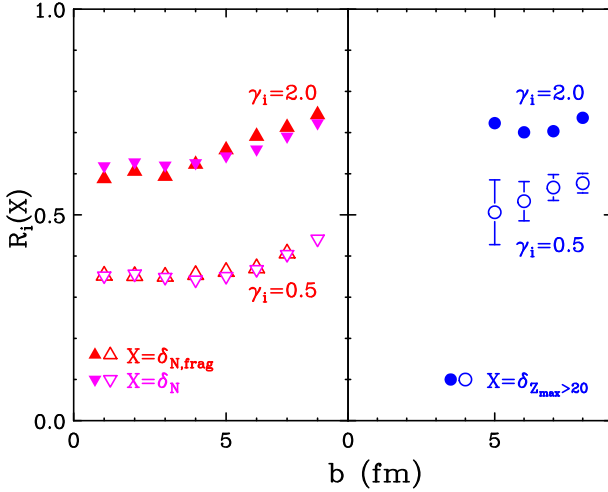


FIG. 7: (Color online) (Left panel) Isospin transport ratios as a function of impact parameters with two tracers. Upright triangle symbols are for the tracer defined by the isospin asymmetry of fragments and unbound nucleons with velocity cut ($v > 0.5v_{beam}^{c.m.}$), $X = \delta_{N,frag}$. Inverted triangles are for the tracer defined by the isospin asymmetry of nucleons with velocity cut ($v > 0.5v_{beam}^{c.m.}$), $X = \delta_N$. (Right panel) The isospin transport ratio as a function of impact parameter with tracer defined by the heaviest fragments with $Z_{max} \geq 20$ in projectile region, $X = \delta_{Z_{max} \geq 20}$.

The R_i values obtained from both tracers as a function of impact parameters are plotted in the left panel of Fig.7. The values of R_i weakly depend on the impact parameters from central collisions to mid peripheral collisions. More importantly, the isospin equilibrium and global thermal equilibrium are not reached even for central collisions. In the ImQMD model, the effective interaction is not sufficiently strong to stop projectile and target nor are the collisions sufficiently frequent because most of them are Pauli suppressed. These two effects keep the reaction system from attaining isospin equilib-

rium even in central collisions. With impact parameter increasing from mid peripheral collisions to peripheral collisions, the number of nucleons transferred from projectile and target decreases quickly causing the R_i values to increase rapidly for $b > 5fm$.

The third tracer uses the isospin asymmetry of heaviest fragments with charge $Z_{max} > 20$ in the projectile region. This tracer is valid mainly for peripheral collisions as the central collisions are dominated by multifragmentation and very few large projectile fragments survive. The dependence of R_i for impact parameter $b > 5fm$ is shown in the right panel of Figure 7. Interestingly, the isospin transport ratios shown in the left and right panels with different isospin tracers have different values especially in the case of ($\gamma_i = 0.5$). Stronger isospin equilibration (smaller R_i values) are observed in the isospin transport ratios $R_i(X = \delta_{N,frag})$ constructed from nucleons and fragments than $R_i(X = \delta_{Z_{max} \geq 20})$ constructed from the heaviest fragments with $Z_{max} \geq 20$. Since isospin diffusion mainly occurs through the low-density neck region, and few target nucleons diffuse to the projectile residues or vice versa due to the short isospin diffusion time at $E/A = 50MeV$, larger $R_i(X = \delta_{Z_{max} \geq 20})$ values result. In contrast, rupture of the neutron-rich neck leads to neutron-rich fragments at mid rapidity. Due to the Fermi motion of nucleons, there is more mixing of emitted nucleons from the target and projectile regions. This leads to small R_i with tracer $X = \delta_{N,frag}$. Experiments [38] have been proposed in both Rare Isotope Beam Factory at RIKEN and the Coupled Cyclotron Facility at NSCL to test these predictions by comparing the isospin transport ratios obtained from residues and from intermediate mass fragments.

Since fragments are formed from the mid rapidity to near projectile rapidity regions, the rapidity dependence of R_i should contain more information on the reaction dynamics. It can provide constraints on the density dependence of symmetry energy. Fig.8 shows R_i as a function of the scaled rapidity y/y_{beam} . The symbols in the left-most panel are data obtained in Ref.[18] for three centrality gates. The isospin tracer $X = \ln(Y(^7Li)/Y(^7Be))$ where $Y(^7Li)/Y(^7Be)$ is the yield ratios of the mirror nuclei, 7Li and 7Be [18]. As expected the values of R_i obtained from peripheral collisions (solid upright triangles) are larger than those obtained in central collisions (solid inverted triangles). For comparisons, the results of $R_i(X = \delta_{N,frag})$ at impact parameters $b = 2, 4, 6$ and $8fm$ are plotted as lines in the middle and right panels. The middle panel contains the results from the soft symmetry potential ($\gamma_i = 0.5$) while the right panel shows the results from the stiff symmetry potential ($\gamma_i = 2.0$). The impact parameter trends and magnitude of the data are more similar to the results of the calculations from soft symmetry potentials ($\gamma_i = 0.5$), consistent with previous analysis [26]. However, the experimental trend of R_i gated with the most central collisions (inverted triangles) are not reproduced by the calculations. The experimental data indicate more equilibrations for central

collisions near mid rapidity while the transport model indicates more transparency. To explore if the different trends of R_i exhibited by the central collisions data are the results from the impact parameter smearing, we have performed multiplicity gated analysis similar to the experimental analysis; the results are similar with larger error bars due to limitations on statistics.

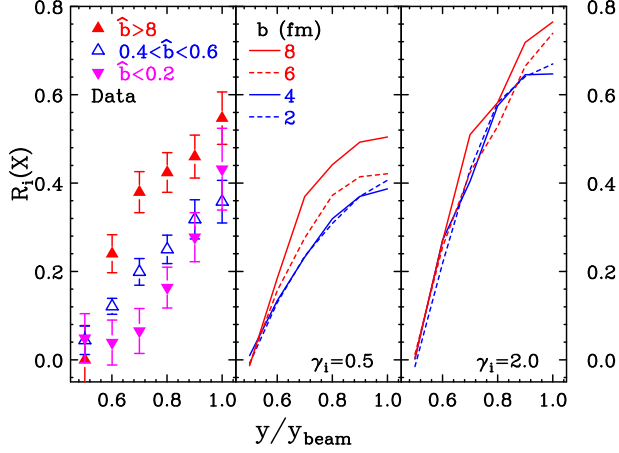


FIG. 8: (Color online) (Left panel) The data of R_i as a function of rapidity for three centrality gates [16]. (Middle panel) The calculated results of $R_i(X = \delta_{N,frag})$ as a function of rapidity for $b = 2, 4, 6, 8 fm$ for $\gamma_i = 0.5$ (Right panel) and $\gamma_i = 2.0$.

Next, we will discuss the influence of different isospin dependence of in-medium nucleon-nucleon cross section on isospin diffusion. Fig.9 shows the isospin diffusion values R_i calculated from three cases of in-medium NN cross sections, 1) normal case, $\sigma_{nn/np}^* = (1 - 0.2\rho/\rho_0)\sigma_{nn/np}^{free}$ (open squares); 2) $\sigma_{nn/np}^* = \sigma_{nn/np}^{free}$ (inverted triangles); 3) isospin independent case, $\sigma_{nn}^* = \sigma_{pp}^* = \sigma_{np}^*$ (solid circles). The isospin tracer adopted here is the $X = \delta_{N,frag}$ using the isospin asymmetry of fragments and unbound nucleons with $v > 0.5v_{beam}^{c.m.}$. Similar to the conclusion of Ref [19], larger in-medium NN cross sections enhance the isospin diffusion ability. But the influence is weak at the energy we studied. Two reasons lead to this conclusion. The dynamical process of heavy ion collisions is governed more by the mean field than the nucleon-nucleon collisions at 50 MeV per nucleon. In addition, the nucleon-nucleon collision frequency is small for peripheral collision. The effects of different in-medium NN cross section dependence on R_i in the ImQMD model are smaller than those predicted by the IBUU04 model, especially for the stiff symmetry potential. This small difference between these two calculations could be caused by the difference on the total nucleon-nucleon collision number in the simulations. In any case, both of these transport models illustrate that the isospin diffusion depends strongly on the symmetry potential and less strongly on the isospin dependence of the in-medium NN cross section at this

beam energy.

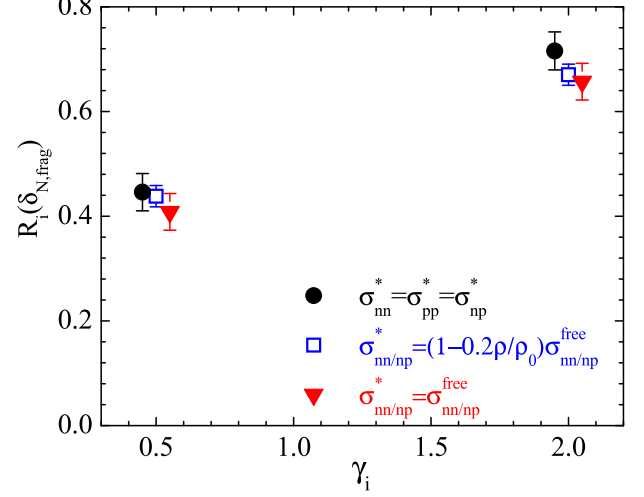


FIG. 9: (Color online) The effects of different in-medium NN cross sections on $R_i(X = \delta_{N,frag})$. The open squares are for the isospin-dependent in-medium NN cross section with phenomenological formula $\sigma_{nn/np}^* = (1 - 0.2\rho/\rho_0)\sigma_{nn/np}^{free}$, (case 1 in text). The inverted triangles are for the free space NN cross section (case 2) $\sigma_{nn/np}^* = \sigma_{nn/np}^{free}$. The solid circles are for the isospin-independent in-medium NN cross section (case 3) $\sigma_{nn}^* = \sigma_{pp}^* = \sigma_{np}^*$.

IV. SUMMARY

In summary, we investigate the influences of the density dependence of symmetry energy, in-medium nucleon-nucleon cross section and impact parameters on isospin observables predicted by the ImQMD model, the reaction dynamics is influenced more by the mean field than the NN collision. The double n/p yield ratios (DR(n/p)) and the isospin transport ratios (R_i) are more sensitive to the density dependence of symmetry energy than the isospin dependence of the in-medium NN cross section. We also examine the impact parameter dependences of the DR(n/p) ratio and isospin transport ratio. Our results illustrate that there is a weak impact parameter dependence of DR(n/p) from central to peripheral collisions, and weak impact parameter dependence of R_i from central to mid-peripheral collisions. From mid-peripheral to peripheral collisions, the R_i increase rapidly with increasing impact parameter due to the decreasing number of transferred nucleons between projectile and target in peripheral collisions.

Cluster formation is important for intermediate energy heavy ion collisions, and the clusters are formed from mid rapidity to projectile or target rapidity as described in the QMD type model. R_i as a function of rapidity describe the data better with soft asymmetry terms. Our results also predict that the values of R_i with the tracer $X =$

$\delta_{Z_{max} \geq 20}$ is larger than R_i with tracer $X = \delta_{N,frag}$ for large symmetry energy at sub-saturation densities (small γ_i); this result can be tested experimentally.

Acknowledgments

This work has been supported by the Chinese National Science Foundation under Grants 10675172, 10979023, 10175093, 10235030 and the U.S. National Science Foundation under Grants PHY-0216783, 060007, 0800026, the High Performance Computing Center (HPCC) at Michigan State University and the Texas Advanced Computing Center, University of Texas.

Appendix

An explicit momentum-dependent interaction term introduced in Eq.(5) changes the mean field potential and therefore the EoS obtained with Skyrme interaction parameters. In order to recover the Equation of State (EoS) obtained with Skyrme interaction parameters and see its influence, we can add a counter term in the explicit momentum-dependent interaction energy density form in Eq.(5) as follows.

$$u_{md} = \frac{1}{2\rho_0} \sum_{N_1, N_2} \frac{1}{16\pi^6} \int d^3p_1 d^3p_2 f_{N_1}(\vec{p}_1) f_{N_2}(\vec{p}_2) 1.57[\ln(1 + 5 \times 10^{-4}(\Delta p)^2)]^2$$

$$-\frac{1}{2\rho_0} \sum_{N_1, N_2} \frac{1}{16\pi^6} \int^{p_f} d^3p_1 d^3p_2 f_{N_1}(\vec{p}_1) f_{N_2}(\vec{p}_2) 1.57[\ln(1 + 5 \times 10^{-4}(\Delta p)^2)]^2 \quad (\text{A.1})$$

With this correction on the momentum-dependent interaction, we repeat the simulations of the Sn + Sn collisions, albeit with less statistics, the results of the mass/charge distribution, neutron/proton ratios and isospin transport ratios from ImQMD are the same as the results obtained using Eq. (5) without the correction term, within statistical uncertainties. The reason is as follows: It is known that the momentum-dependent interaction plays an essential role in the overlap region of the projectile and targets in HICs. Particles with larger relative momenta are positioned more closely in space and the strong repulsive force from the momentum-dependent interaction causes the system to have a lower maximal compression and increases the mean free path in this lower compressed region. Thus, the strength of the repulsive force from the Momentum Dependent Interaction (MDI) and the NN collision frequency related to the mean free path influence the observables of HICs directly. However at $E/A = 50 \text{ MeV}$, the relative momentum of nucleons is not large enough and the frequency of nucleon-nucleon collisions are suppressed by the Pauli blocking effects. Therefore, the two different Momentum Dependent Interactions in Eq.(5) and Eq.(A.1) do not lead to large difference of the observables.

-
- [1] J. Lattimer and M.Prakash, Ap. J., 550, 426 (2001).
 - [2] J. Lattimer and M.Prakash, Science, 304, 536 (2001).
 - [3] A. Steiner and et al., Phys. Rep., 411, 325 (2005).
 - [4] A. L. Watts and T. E.Strohmayer, Astr. J., 637, L117 (2006).
 - [5] D.G.Yakovlev and C.J.Pethick, Annu. Rev. Astron. Astrophys., 42, 169 (2004).
 - [6] B.A.Brown, Phys. Rev., C43, R1513 (1991).
 - [7] B. Li and et al., Phys. Rep, 464, 113 (2008).
 - [8] P.Danielewicz, R.Lacey, and W.G.Lynch, Science, 298, 1592 (2006).
 - [9] C.Fuch and H.Wolter, Eur. Phys. J., A30, 5 (2006).
 - [10] U. Garg, Nucl. Phys., A731, 3 (2004).
 - [11] H.S.Xu and et al., Phys.Rev.Lett., 85, 716 (2000).
 - [12] M.B.Tsang and et al., Phys.Rev.Lett., 86, 5023 (2001).
 - [13] D.V.Shetty and et al., Phys.Rev., C70, 011601 (2004).
 - [14] M.B.Tsang, T.X.Liu, L.Shi, and et al., Phys.Rev.Lett., 92, 062701 (2004).
 - [15] L.-W. Chen, C. M. Ko, and B.-A. Li, Phys.Rev.Lett., 94, 032701 (2005).
 - [16] Q. Li, Z. Li, and et al., Phys.Rev.C., 72, 034613 (2005).
 - [17] Q. Li, Z. Li, and et al., Phys.Rev.C., 73, 051601 (2006).
 - [18] T.X.Liu, W.G.Lynch, M.B.Tsang, and et al., Phys.Rev., C76, 034603 (2007).
 - [19] B.-A. Li and L.-W. Chen, Phys.Rev., C72, 064611 (2005).
 - [20] M.A.Famiano, T. Liu, W.G.Lynch, and et al., Phys.Rev.Lett., 97, 052701 (2006).
 - [21] B. Li, C. Ko, and Z. Ren, Phys.Rev.Lett., 78, 1644 (1997).
 - [22] B. Li, L.W.Chen, G.C.Yong, and W.Zuo, Phys.Lett., B634, 378 (2006).
 - [23] B. Li, Phys.Rev.Lett., 85, 4221 (2000).
 - [24] B. Li, Nucl. Phys., A734, 539c (2004).
 - [25] G. Yong, B. Li, and L. Chen, Phys.Rev., C73, 034603 (2006).
 - [26] M.B.Tsang, Y. Zhang, P.Danielewicz, M.Famiano, Z. Li, W.G.Lynch, and A.W.Steiner, Phys.Rev.Lett., 102, 122701 (2009).
 - [27] B. Giordano, M. Colonna, M. D. Toro, and et al., Phys.Rev.C., 81, 044611 (2010).
 - [28] P. Napolitani, M. Colonna, and et al., Phys.Rev.C., 81, 044619 (2010).
 - [29] J.Aichelin, Phys.Rep., 202, 233 (1991).
 - [30] Y. Zhang, P.Danielewicz, M.Famiano, Z. Li, W.G.Lynch, and M.B.Tsang, Phys.Lett., B664, 145 (2008).
 - [31] Y. Zhang and Z. Li, Phys.Rev., C71, 024604 (2005).
 - [32] Y. Zhang and Z. Li, Phys.Rev., C74, 014602 (2006).
 - [33] Y. Zhang, Z. Li, and P. Danielewicz, Phys.Rev., C75, 034615 (2007).
 - [34] J. Aichelin, A. Rosenhauer, G. Peilert, H. Stocker, and W. Greiner, Phys.Rev.Lett, 58, 1926 (1987).
 - [35] J. J.Cugnon, D.L'Hôte, Nucl.Instr.Meth.Phys., B111,

- 215 (1996).
- [36] R. Nebauer, J. Aichelin, and the INDRA collaboration, Nucl.Phys., A658, 67 (1999).
- [37] A. Ono, P. Danielewicz, W. A. Friedman, W. G. Lynch, and M.B.Tsang, Phys.Rev., C68, 051601(R) (2003).
- [38] "NSCL experiment 07038,"